The Journal of the Korean Society of Oceanography
Vol. 30, No. 4, pp. 288-301, August 1995

Rates of Sediment Accumulation and Particle Mixing in the KODOS Site of the Clarion-Clipperton Fracture Zones

DEOK SOO MOON AND KEE HYUN KIM
Dept. of Oceanography, Chungnam National University, Taejon 305-764, Korea

클라리온-클리퍼톤 균열대 KODOS 지역 퇴적물의 퇴적율과 입자혼합율

문덕수, 김기현
충남대학교 해양학과, 대전 305-764

Rates of the sedimentation and particle mixing have been estimated by applying uranium-series disequilibrium techniques to three sediment cores collected from the Korea Deep Ocean Study (KODOS) site between the Clarion and Clipperton Fracture Zones (CCFZ) of the Equatorial Pacific.

Sedimentation rates based on the profiles of excess ^{230}Th activity and $^{230}Th_{xs}/^{232}$Th activity ratios at the southeastern part of the study area were estimated to be in the order of a few millimeters per thousand year, while at the northwestern part a factor of ten lower. Excess activities of ^{230}Th and $^{230}Th_{xs}/^{232}$Th ratios showed intervals of constant values in the upper part of the sediment cores, probably generated by biological particle mixing.

A "two-box" advection-diffusion steady state mixing model was employed in order to estimate particle mixing rates in the upper and the lower layers, based on the distribution profiles of excess ^{210}Pb activities. Particle mixing coefficients were estimated to be in the order of 10^1 cm^2/y in the upper layer and 10^{-1}-10^0 cm^2/y in the lower layer.

적도 태평양 클라리온-클리퍼톤 균열대 사이의 한국심해 연구(KODOS) 지역에서 채취된 3개의 퇴적물 코아에 우라늄계열 비평형 기법을 적용하여 퇴적율과 입자교란율이 추정되었다.
과잉 토륨-230 방사능과 과잉 토륨-230/토륨-232 방사능비의 수직분포로부터 추정된 퇴적율은 연구지역의 남동부 지역에서 천년당 수 밀리미터로 추정되었으며, 북서부에서는 천년당 일 밀리미터 이하로 추정되었다. 퇴적물 시료의 상부에서 과잉 토륨-230 방사능과 과잉 토륨-230/토륨-232 방사능비가 일정한 수직분포를 보이며 이는 저서생물등에 의한 입자 교란작용의 영향인 것으로 사료된다.

과잉 납-210의 수직농도 분포를 근거로 퇴적물 상부층과 하부층의 입자교란 속도를 추정하기 위하여 "2상자" 이류-확산 입자혼합 모델을 이용하였다. 입자혼합계수는 상부층에서는 수 10 cm^2/y이며 하부층에서는 일 내지 수 cm^2/y로 추정되었다.

INTRODUCTION

Uranium exists in seawater as stable complex ions of uranyl carbonates, $UO_2(CO_3)_3^{4-}$ and $UO_2(CO_3)_2^{2-}$, whereas thorium is characterized by its high particle reactivity in the ocean. ^{230}Th and ^{232}Th have different geochemical pathways due to their different origin: ^{232}Th enters the oceans primarily in detrital form, whereas ^{230}Th is formed continuously by the decay of its parent ^{234}U dissolved in seawater, and quantitatively removed from seawater via particle scavenging, resulting in the accumulation in deep-sea sediments as unsupported activities.

In pelagic ocean, most of excess ^{210}Pb in the sed-

Table 1. Location, water depth (m) and sea-bottom feature of sediment cores

Station	Sediment Sample I.D.	Location		Water Depth(m)	Topography	Bottom sediment
		Latitude(N)	Longitude(E)			
KODOS89-15	BX-89-15	9° 20′	152° 40′	5212	Abyssal plain	Radiolaria bearing clay
KODOS90-01	BX-80-01	7° 38′	146° 09′	5270	Abyssal plain	Radiolaria bearing clay
KODOS9-36	BX-90-36	10° 30′	151° 44′	5075	seamount	Siliceous clay

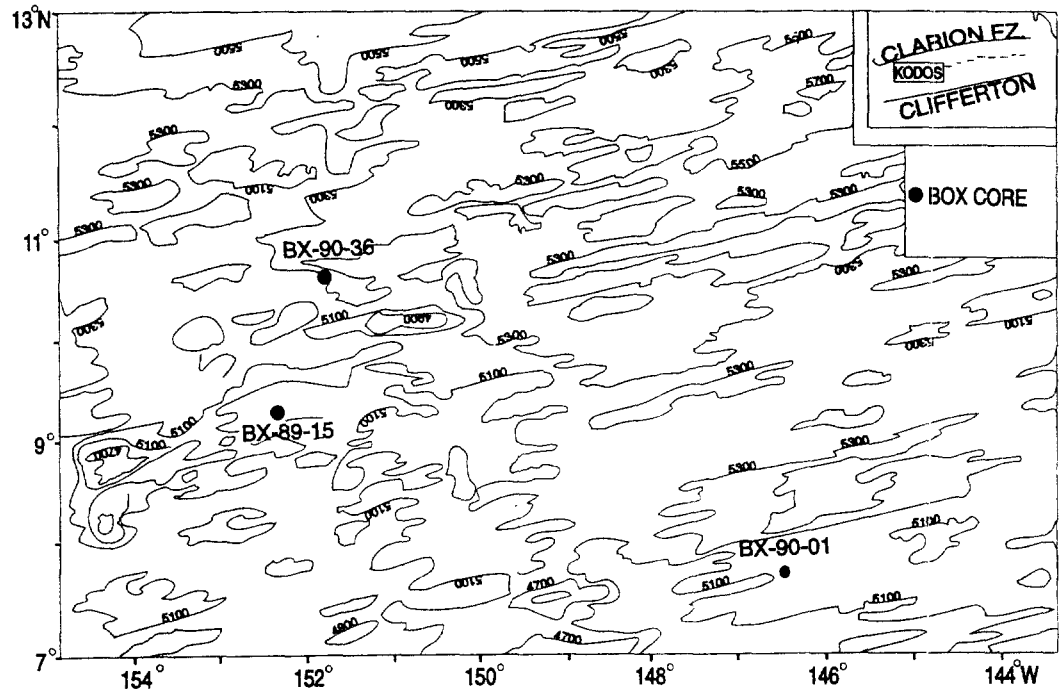

Fig. 1. Bathymetry map of KODOS area showing the location of box cores analyzed in this study. Water depth in meters.

iment originates from the decay of atmospheric ^{222}Rn and of ^{226}Ra in seawater (Goldberg, 1963; Cochran, 1982; Krishnaswami *et al.*, 1980). The ^{210}Pb in seawater from these sources is scavenged by sinking particulates of both biogenic and detrital origin throughout the water column.

Owing to its half-life of 22.3 years, ^{210}Pb has been proved to be an important nuclide for the study of particle mixing processes in surface sediments (Krishnaswami *et al.*, 1980; Benninger and Krishnaswami, 1981; DeMaster and Cochran, 1982; Kim and Burnett, 1988). The particle mixing can affect the chemical diagenesis of sediment by extending the oxidizing zone (Aller and Cochran, 1976) and the processes leading to the formation of manganese nodules (Piper and Fowler, 1980).

Korea Ocean Research and Development Institute (KORDI) surveyed the area of 200,000 km^2 in the Clarion-Clipperton Fracture Zone (CCFZ) and collected manganese nodules and sediment cores (KORDI, 1986; 1987; 1990; 1992). Jeong *et al.* (1988) reported that sedimentary layers in KODOS site progressively become thin toward north. Sedimentation rates in the KODOS site were estimated to be 0.2 mm/ky by biostratigraphy and Magnetic property (KORDI, 1991).

The purpose of this study is to estimate the rates of sedimentation and biological particle mixing in order to understand sedimentary environments of the KODOS sites in the equatorial Pacific. Results

from this study will serve as a basic information about sedimentary environments of the area.

MATERIALS AND METHODS

Field work

Samples analyzed in this study were collected from the KODOS sites of the northeastern part of the central equatorial Pacific, during the R/V Farnella cruise in 1989 and 1990 by KORDI (Korea Ocean Research and Development Institute) team, and supplied to us in 1992. The location and water depth of the sampling sites are presented in Table 1 and Fig. 1 (KORDI, 1990; 1991).

Manganese nodules and sediment cores were sampled in undisturbed state using a box corer. Immediately after the corer was retrieved onto the deck, seawater overlying the sediment was carefully removed by siphoning to describe condition of manganese nodules and sediment surface. After handpicking of manganese nodules, subcores were carefully collected by inserting clear acrylic pipes (diameter 8 cm) into the sediment by hand. Retrieved subcores were preserved in a refrigerator until analysis.

Analytical methods

Figure 2 shows a flow of the analytical scheme adapted in this study. After slabs were obtained from cores using acrylic box, X-radiographs were taken to see the bioturbation structure in box core sediments.

After taking X-radiographs, sediment slabs were sectioned at an interval of 1 cm. The dried samples were ground into powder, weighed, loaded into plas-

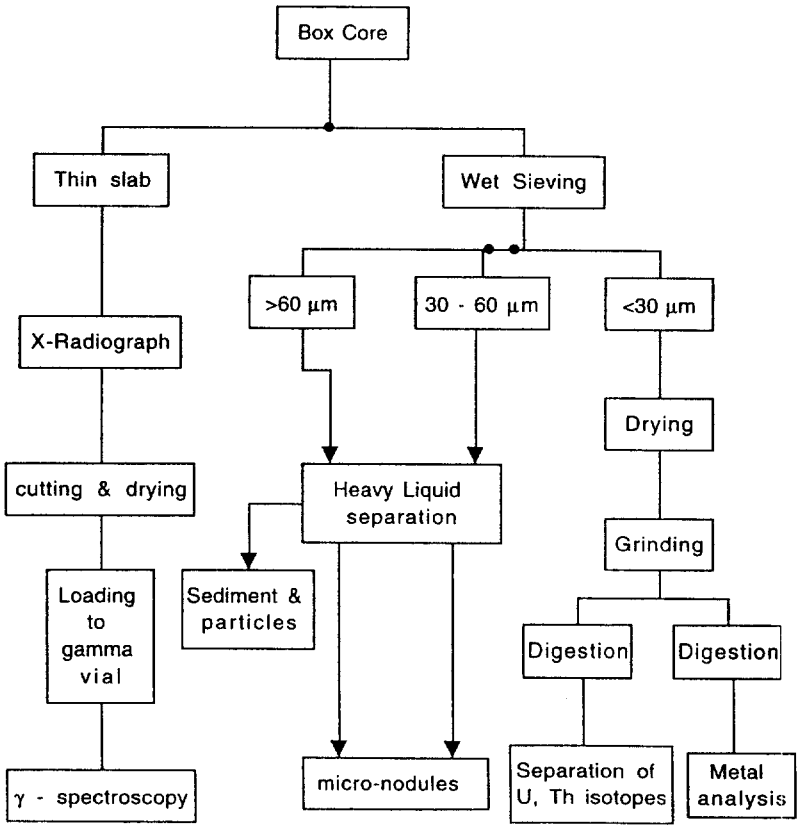

Fig. 2. Flow diagram for the sediment analysis.

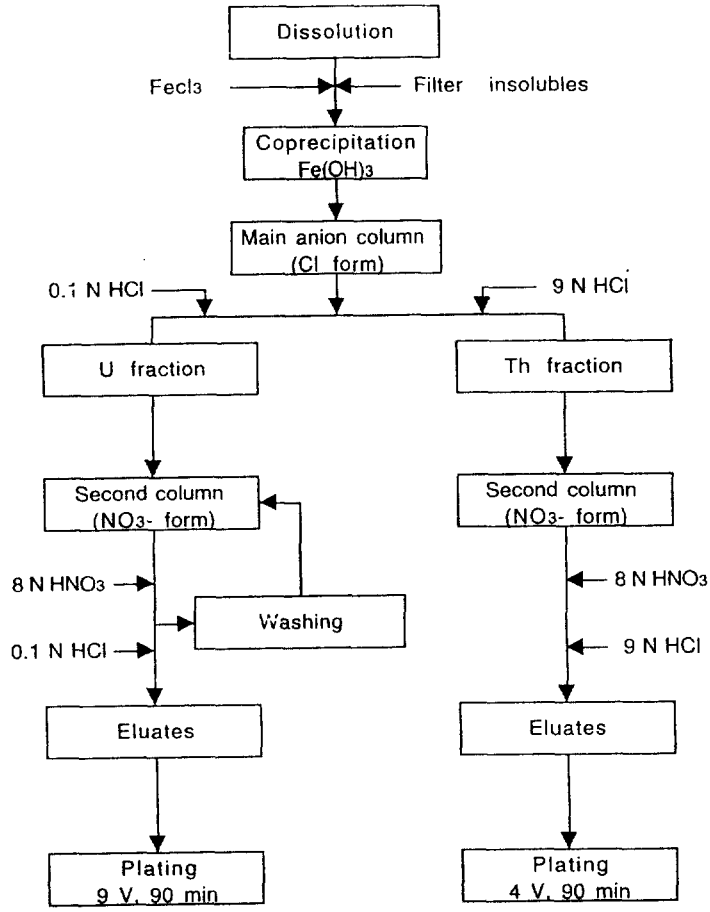

Fig. 3. Separation scheme of uranium and thorium in sediment samples (Anderson and Fleer, 1982).

tic counting vials and sealed air-tightly with epoxy glue. The samples were aged for 4 weeks to ensure the equilibrium between ^{226}Ra and its daughter nuclide ^{222}Rn (Kim and Burnett, 1983).

The sediment samples remaining after making X-radiograph slabs were wet-sieved with deionized distilled water (DDW) using nylon sieves in order to divide three size classes, <30 μm, 30-60 μm and >60 μm. Fractions coarser than 30 μm contain mainly a radiolarian tests and micronodules of Fe and Mn oxides, whereas fraction finer than 30 μm mostly sediment particles. Each fraction was centrifuged and dried in an oven at 60 for several days. The fraction finer than 30 μm were ground in an agate mortar and kept to analyze the isotopes of uranium and thorium.

Activities of ^{226}Ra and ^{210}Pb were determined by gamma-ray spectroscopy utilizing a well-type intrinsic germanium detector. Details of the nondestructive gamma-ray spectrometric measurements can be found elsewhere (Kim and Burnett, 1983; 1985).

Isotopes of U and Th in sediment were determined by modified procedures previously described by Anderson and Fleer (1982) and Huh (1982). Figure 3 shows a separation scheme of U and Th nuclides employed in this study. Briefly, sediment samples (0.5-1.0 g) were weighed, combusted at 550°C for 12 hour in a muffle furnace, spiked with 1 ml of ^{232}U/^{228}Th yield tracer (11.66 dpm ^{232}U/ml), digested with a mixture of HCl and HNO_3 (*aqua regia*) in the presence of perchloric acid, and filtered using membrane filter paper (pore size: 0.45 μm). Uranium and thorium were separated from each

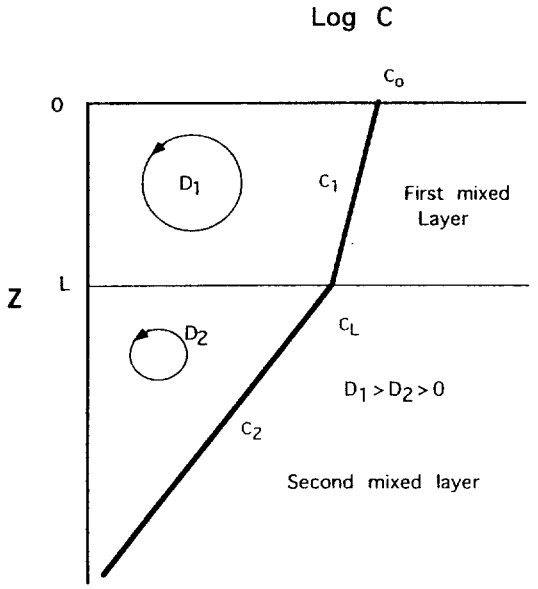

Fig. 4. Schematic diagram explaining the two-box mixing model employed in this study. C=activity of radionuclide; D_1=mixing coefficient for the first box; D_2=mixing coefficient for the second box; z=depth in core; L=thickness of the first mixed layer.

other by anion exchange techniques utilizing Dowex AG1-X8 resin (100-200 mesh: chloride form).

For further purification of uranium and thorium, two types of resin were used: the first column filled with untreated AG1 resin of chloride form and second column packed with nitrate-form resin prepared from chloride one following the procedures of Joshi (1984). The purified uranium were electroplated for 60-90 min. at 9 volts and thorium at 4 volts for the same time onto stainless steel planchets.

Counting of uranium and thorium isotopes was done by alpha spectrometry with silicon surface-barrier detectors (Canberra) with an active surface area of 450 mm^2 and a minimum depletion thickness of 100 microns.

Mathematical model of particle mixing

A "two-box" advection-diffusion particle mixing model is used to estimate the rates of sedimentation and particle mixing. "One-box" mixing model has been widely used in most of previous studies on deep sea sediment (Goldberg and Koide, 1962; DeMaster and Cochran, 1982; Cochran, 1985; Aller and DeMaster, 1984). However, in cases where bioturbation occurs deeply in sediment, two-box model is appropriate to study particle mixing (Kim and Burnett, 1988). In our sediment cores consisted of layers with two distinctive slopes in excess ^{210}Pb profiles, significant activities of excess ^{210}Pb were observed down to the depths of 30 cm, which can not be explained by one-box model.

We supposed that within the first (upper) box particle mixing is relatively fast and that within the second (lower) box, mixing is slower than the above layer (Fig. 4). The model equation governing the distribution of the excess 210Pb within the first box is:

$$\frac{dC_1}{dt} = D_1\left(\frac{\partial^2 C_1}{\partial z^2}\right) - S\left(\frac{\partial C_1}{\partial z}\right) - \lambda C_1 = 0 \qquad (1)$$

and within the second box:

$$\frac{dC_2}{dt} = D_2\left(\frac{\partial^2 C_2}{\partial z^2}\right) - S\left(\frac{\partial C_2}{\partial z}\right) - \lambda C_2 = 0 \qquad (2)$$

where the subscripts represent the first (1) and the second (2) box; z=depth below the sediment surface (cm); C=the excess activity (dpm/g); λ=the decay constant of the radionuclide (^{210}Pb=0.0311 y^{-1}); D= the particle mixing coefficient (cm^2/y); S=sedimentation rate (cm/y). A general solution of equations (1) and (2) is :

$$C_i = P_i \exp(A_i z) + Q_i \exp(B_i z) \qquad (3)$$

where, $A_i = (S + \sqrt{S_2 + 4D_i\lambda})/2D_i$;

$B_i = (S - \sqrt{S_2 + 4D_i\lambda})/2D_i$,

the subscripts (i=1 or 2) represent the first or the second box, and P and Q are constants.

With the following four boundary conditions;

1) Initial activity: $C_1 = C_o$ at z=0

2) Activity continuity: $C_1 = C_2$ at z=L

3) Flux continuity : $-D_1\left(\partial\frac{C_1}{\partial} z\right) - D_2\left(\partial\frac{C_2}{\partial} z\right)$ at z=L

Table 2. Results of radiochemical determination of U and Th nuclides in sediment sample BX-90-36 (10°30′N, 151°44′E; water depth 5,075 m). Ratios are activity ratios and errors quoted are 1σ errors based on counting statistics.

Depth (cm)	^{238}U (ppm)	^{232}Th (ppm)	^{230}Th (dpm/g)	^{230}Th$_{xs}$ (dpm/g)	^{230}Th$_{xs}$/^{232}Th Activity ratio
0-1	0.80±0.10	11.4±0.74	143±3.54	142±3.54	50.9±3.56
4-6	0.72±0.11	8.55±0.49	132±2.53	131±2.53	62.4±3.79
9-10	1.20±0.14	10.1±0.63	131±3.03	130±3.03	52.3±3.51
14-15	1.11±0.09	10.8±0.55	122±3.13	120±3.13	45.3±2,57
19-20	0.87±0.09	10.8±0.56	69.4±1.41	68.5±1.41	25.7±1.42
24-25	1.43±0.09	7.40±0.37	3.52±0.13	2.42±0.11	1.33±0.09
29-30	1.30±0.14	8.81±0.74	3.19±0.23	1.79±0.26	0.83±0.14
34-35	1.76±0.10	9.29±0.34	1.50±0.07	0.33±0.10	0.14±0.04
39-40	1.14±0.12	9.79±0.53	2.60±0.14	1,51±0.17	0.63±0.08
44-45	1.41±0.08	10.5±0.86	1.53±0.16	0.49±0.17	0.19±0.07

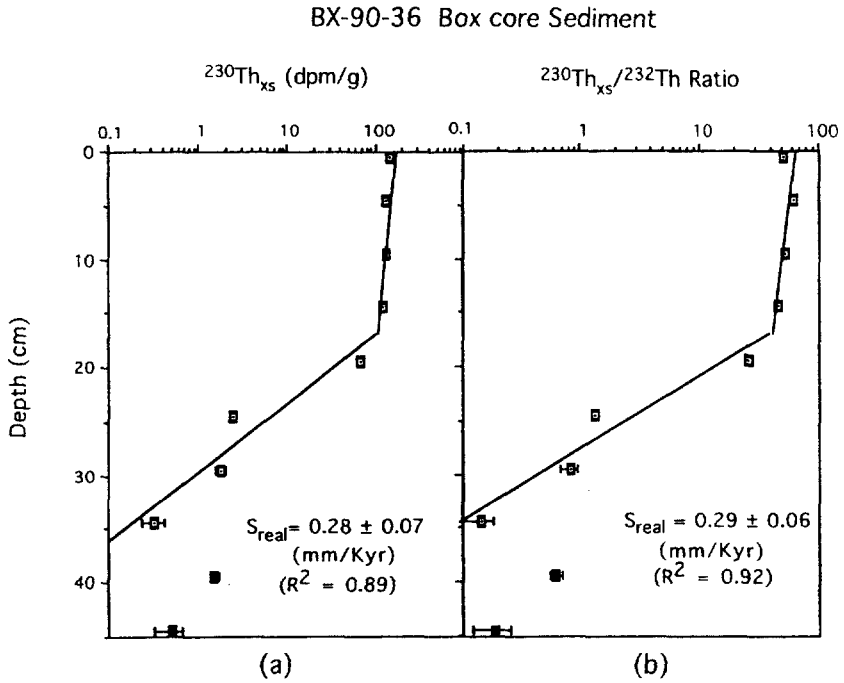

Fig. 5. Plots of ^{230}Th$_{xs}$ activity (a) and ^{230}Th$_{xs}$/^{232}Th activity ratio (b) as a function of depth at BX-90-36 core. *Solid boxes* represent ^{230}Th$_{xs}$ (a) and ^{230}Th$_{xs}$/^{232}Th (b) data points not included in regression.

4) Zero excess activity at infinite depth : $C_2 \rightarrow 0$ as $z \rightarrow \infty$

where, L = the depth of transition between the first and second mixed layers.

We can obtain an analytical solution for equation (1) and (2). Detailed explanation for this model will be found in Kim and Burnett (1988). The relationship between the *apparent* (S_{app}) and *"real"*(S) sedimentation rates and D_2 are given by:

$$-\left(\frac{\lambda}{S_{app}}\right)=(S-\sqrt{S^2+4D_2\lambda})/2D_2$$

Solving this equation for D_2, we obtain the following equation:

$$D_2=(S_{app}*(S_{app}-S))/\lambda \quad (4)$$

RESULTS AND DISCUSSION

Excess activity of ^{230}Th (^{230}Th$_{xs}$) and activity ratios

Table 3. Activities of radionuclides, ^{210}Pb (total), ^{226}Ra and excess $^{210}Pb_{xs}$=^{210}Pb-^{226}Ra), from the sediment core BX-90-36. Errors quoted are 1σ errors based on counting statics.

Depth (cm)	^{210}Pb (dpm/g)	^{226}Ra (dpm/g)	$^{210}Pb_{xs}$ (dpm/g)
0-1	83.4±1.96	46.3±0.56	37.1±2.04
4-5	78.4±1.75	53,2±0.55	25.3±1.83
9-10	84.9±2.05	62.4±0.68	22.5±2.16
15-16	82.3±1.55	63.3±0.52	19.0±1.63
17-18	65.9±1.37	47.7±0.44	19.0±1.63
19-20	53.9±1.45	37.8±0.47	18.2±1.44
22-23	58.7±1.40	44.1±0.46	17.6±1.56
25-26	26.7±1.05	15.7±0.30	14.7±1.47
29-30	14.1±0.81	10.2±0.24	11.0±1.09
32-33	12.1±0.93	8.99±0.27	3.95±0.84

of $^{230}Th_{xs}/^{232}Th$ in sediments decrease exponentially with the depth (where, $^{230}Th_{xs}$=$^{230}Th_{total}$-^{234}U). The decrease of $^{230}Th_{xs}$ and $^{230}Th_{xs}/^{232}Th$ ratio in cores can be used to estimate the sedimentation rates, assuming: (1) that ^{230}Th production rate in water column is constant (Broecker and T.H. Peng, 1982) and (2) that the sedimentation rate is constant over a dating interval of interest. Since the chemical behaviour of ^{230}Th during sediment diagenesis is similar to that of ^{232}Th, the use of normalized ratios of $^{230}Th_{xs}/^{232}Th$ to estimate sedimentation rate may be preferable to $^{230}Th_{xs}$ activity alone.

The depth of the surface mixed layer in deep sea sediments has been observed less than 10 cm from the sediment surface in previous studies of particle mixing (Goldberg and Koide, 1962; DeMaster and Cochran, 1982; Cochran, 1985; Aller and DeMaster, 1984). In our cores, excess ^{210}Pb were clearly observed down to depths of 30 cm (Table 3 and 5). This deep penetration of excess ^{210}Pb in the core could be interpreted by deep particle mixing as in the case of $^{239+240}Pu$ in peru margin sediments (Santschi *et al.*, 1986). A change of slopes between two segments of cores can be explained by a two-box model (Kim and Burnett, 1988).

BX-90-36

Core BX-90-36 was retrieved from seamount region of water depth of 5,075 m located in the northwestern part of the KODOS-90 site (KORDI, 1991). Sediment at BX-90-36 chiefly composed of

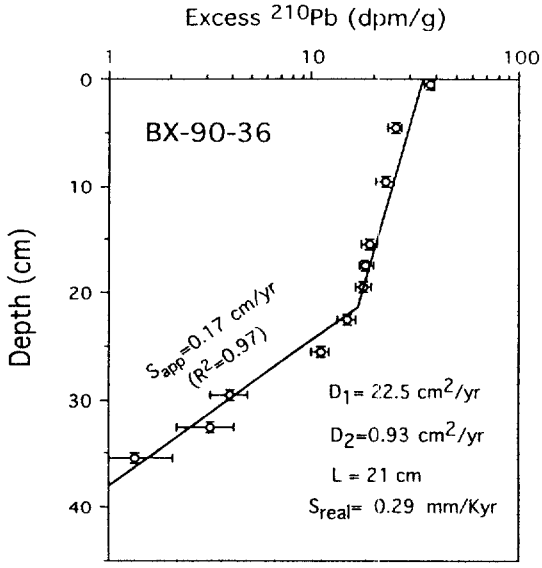

Fig. 6. Excess ^{210}Pb profile for X-90-36. D=particle mixing coefficient, L-thickness of the first mixed layer S_{real}=real sedimentation rates determined by $^{230}Th_{xs}/^{232}Th$ activity, S_{app}=apparent sedimentation rates estimated by excess ^{210}Pb profile in lower layer than SML.

siliceous clay. Exponential decreases of excess ^{230}Th activity and $^{230}Th_{xs}/^{232}Th$ ratio as a function of core depth have been observed in this core (Table 2). The profiles of excess ^{230}Th activity and $^{230}Th_{xs}/^{232}Th$ ratio show flat slopes within the upper layer of sediment (<21 cm), indicating rapid particle mixing (Fig. 5).

In core BX-90-36, excess ^{210}Pb were observed down to depth of 35 cm (Table 3). We interpreted that the deep penetration of excess ^{210}Pb in the core is due to deep particle mixing as in the case of $^{239+240}Pu$ of Santschi *et al.* (1986). A change of slopes between two segments at 21 cm depth may represent the boundary between the first and the second boxes of the two-box model (Fig. 6).

BX-89-15

BX-89-15 core was collected in abyssal plain of water depth of 5,212 m (Fig. 1). Its surface layer was well preserved in the subcore analyzed in this study. The color of sediment above the 10 cm depth in the core was pale brown and dark brown below

Table 4. Results of radiochemical determination of U and Th nuclides in sediment sample BX-89-15 (9°20′N, 152°40′E; water depth 5,212 m). Ratios are activity ratios and errors quoted are 1σ errors based on counting statistics.

Depth (m)	^{238}U (ppm)	^{232}Th (ppm)	^{230}Th (dpm/g)	^{230}Th$_{xs}$ (dpm/g)	^{230}Th$_{xs}$/^{232}Th Activity Ratio
0-1	1.93±0.23	12.2±0.93	154±3.49	152±3.50	50.7±4.04
2-3	1.46±0.17	11.6±0.76	102±2.61	101±2.62	35.2±2.47
4-5	1.62±0.20	9.85±0.66	78,6±1.95	77.2±1.96	31.9±2.29
7-8	1.39±0.16	11.2±0.50	101±1.80	100±1.80	36.5±1.77
9-10	0.93±0.08	9.35±0.56	78.6±1.79	77.6±1.79	33.7±2.16
12-13	1.47±0.16	9.68±0.53	52.3±1.14	50.7±1.15	21.3±1.27
14-15	1.57±0.18	8.86±0.44	35.6±0.70	34.1±0.72	15.6±0.85
19-20	1.27±0.11	7.96±0.46	15.3±0.41	14.2±0.42	7.26±0.47
23-24	1.56±0.17	8.50±0.39	19.3±0.39	17.9±0.41	8.56±0.44
29-30	2.18±0.17	5.65±0.28	4.29±0.13	2.61±0.18	1.87±0.16
39-40	1.71±0.15	6.20±0.31	2.85±0.11	1.55±0.15	1.02±0.11
44-45	2.36±0.10	5.51±0.52	6.01±0.31	3.76±0.32	2.77±0.35
49-50	2.37±0.25	6.26±0.42	8.85±0.29	5.67±0.38	3.68±0.35

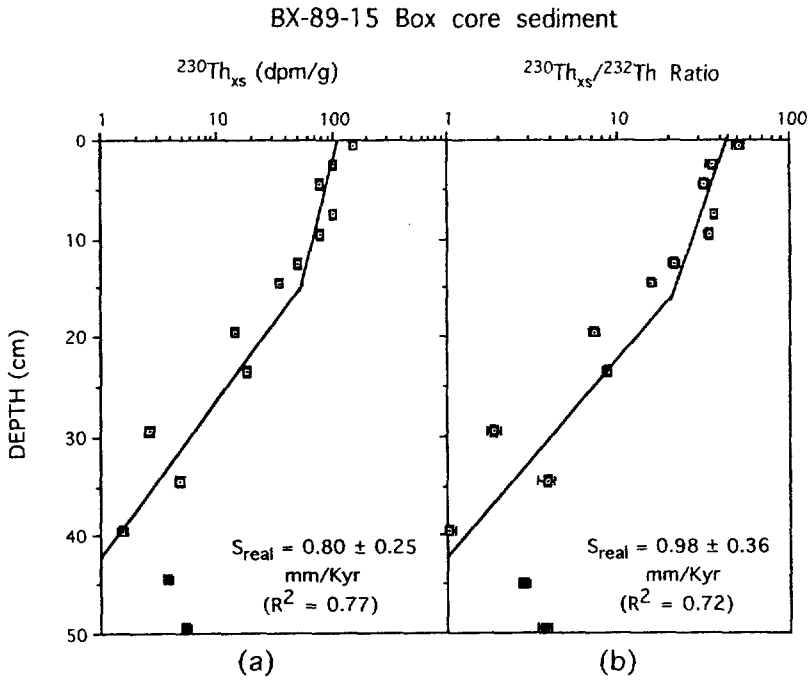

Fig. 7. Plots of ^{230}Th$_{xs}$ activity (a) and ^{230}Th$_{xs}$/^{232}Th activity ratio (b) as a function of depth at BX-89-15 core, ^{230}Th$_{xs}$= ^{230}Th$_{total}$-^{234}U. S=sedimentation rate estimated from all data points, S$_{real}$=real sedimentation rate calculated from data points below SML (18.5 cm), R^2=goodness-of-fit. Error bars refer to 1-σ counting statistics (horizontal) and depth intevals (vertical). *Solid boxes* represent ^{230}Th$_{xs}$ (a) and ^{230}Th$_{xs}$/^{232}Th (b) data points not included in regression.

the depth (Jung, 1991). This color change in sediment is due to hiatus between the Quaternary and the Tertiary sediment (Jeong, 1993).

Figure 7 shows the distribution profiles of ^{230}Th$_{xs}$ and ^{230}Th$_{xs}$/^{232}Th activity ratio in core BX-89-15. ^{230}Th$_{xs}$ activity and ^{230}Th$_{xs}$/^{232}Th ratio decrease exponentially with depth and these patterns indicate that sedimentation rate is constant over the dating interval. Also, the profiles of ^{230}Th$_{xs}$ and ^{230}Th$_{xs}$/^{232}Th indicate that sediment particles are well mixed in the

Table 5. Activities of radionuclides, ^{210}Pb (total), ^{226}Ra and excess ^{210}Pb ($^{210}Pb_{xs}$=^{210}Pb-^{226}Ra), from the sediment core BX-89-15. Errors quoted are 1σ errors based on counting statistics.

Depth (cm)	^{210}Pb (dpm/g)	^{226}Ra (dpm/g)	$^{210}Pb_{xs}$ (dpm/g)
0-1	76.7±1.93	47.9±0.59	28.7±2.02
2-3	76.1±1.78	49.3±0.55	26.8±1.87
4-5	83.4±1.68	59.2±0.55	24.2±1.77
7-8	67.7±1.65	47.2±0.53	20.5±1.73
9-10	51.6±1.42	30.9±0.42	20.7±1.48
12-13	48.7±1.29	31.5±0.40	17.2±1.35
14-15	44.2±1.15	29.1±0.36	15.2±1.12
16-17	30.9±0.97	17.4±0.28	13.4±1.01
18-19	22.8±0.86	11.1±0.23	11.7±0.90
20-21	17.0±0.71	9.91±0.20	7.10±0.74
23-24	11.0±0.54	6.04±0.15	4.98±0.56
26-27	6.99±0.46	4.26±0.13	2.74±0.48
29-30	5.01±0.44	3.83±0.13	1.18±0.46

upper few centimeters. Because $^{230}Th_{xs}$ and $^{230}Th_{xs}$/^{232}Th profiles in the first mixed layer are affected by faster particle mixing than the second layer, the slope of regression line in upper layer is more flat than that of the lower layer.

BX-90-01

BX-90-01 core site is in an abyssal plain of water depth of 5,270 m located in the southeastern part of KODOS-90 area (KORDI, 1990; Jeong *et al.*, 1988). Sediments in this place are consisted of radiolarian bearing clay. Profiles of excess ^{230}Th and $^{230}Th_{xs}$/^{232}Th at BX-90-01 are presented in Fig. 9 (Table 6).

Sedimentation rates

The distribution of $^{230}Th_{xs}$ activity with the depth is given by:

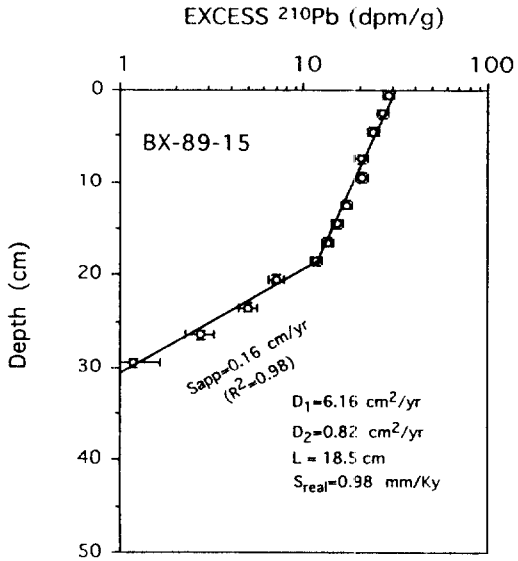

Fig. 8. Excess ^{210}Pb profile for BX-89-15. Error bars refer to 1-σ counting statistics (horizontal) and depth intervals (vertical).

$$(^{230}Th_{xs})_z = (^{230}Th_{xs})_{z=0} * e^{(-\lambda/s)z}$$

Similarly, for $^{230}Th_{xs}$/^{232}Th:

$$(^{230}Th_{xs}/^{232}Th)_z = (^{230}Th_{xs}/^{232}Th)_{z=0} * e^{(-\lambda/s)z}$$

Sedimentation rates were estimated from the slope of the regression line fitted to semi-logarithmic plot of ^{230}Th and $^{230}Th_{xs}$/^{232}Th activity ratios by the following equation:

$$S = -\lambda/a$$

where S is sedimentation rate (mm/ky), a is the slope of best-fit line (cm^{-1}), λ_{230} is the decay constant of ^{230}Th (9.22×10^{-6} y^{-1}) and z is the depth in

Table 6. Results of radiochemical determination of U and Th nuclides in sediment sample BX-90-01 (7°38′N, 146°09′E; water depth 5,270 m). Ratios are activity ratios and errors quoted are 1σ errors based on counting statistics.

Depth (cm)	^{238}U (ppm)	^{232}Th (ppm)	^{230}Th (dpm/g)	$^{230}Th_{xs}$ (dpm/g)	$^{230}Th_{xs}$/^{232}Th Activity ratio
0-1	0.79±0.11	10.9±0.65	151±3.23	150±3.23	55.8±3.51
9-10	0.69±0.09	10.7±0.69	138±3.37	138±3.37	52.4±3.60
19-20	1.04±0.12	10.4±0.79	126±3.50	125±3.50	48.6±3.91
29-30	1.18±0.17	11.3±0.77	117±2.97	116±2.98	41.8±3.04
39-40	1.41±0.12	9.49±0.51	89.2±1.71	87.7±1.71	37.6±2.16
44-45	2.05±0.12	9.79±0.37	51.8±0.95	50.0±0.95	20.9±0.89
49-50	1.46±0.14	9.63±0.60	54.3±1.35	52.9±1.35	22.3±1.50
54-55	0.81±0.06	10.1±0.37	35.6±0.66	34.9±0.66	14.1±0.58

Table 7. Sedimentation rates and biological praticle mixing coefficients estimated for sediment cores from KODOS site.

Sample I.D.	S* (mm/ky)	S_{appt}† (mm/ky)	Mixing rate (cm^2/y)		First layer depth(cm)
			D_1	D_2	L
BX-90-36	0.29±0.06	1700	22.5	0.9	21.0
BX-89-15	0.98±0.36	1600	6.16	0.8	18.5
BX-90-01	1.61±0.49	N.D.	N.D.	N.D.	40.0

*Real sedimentation rates estimated from $^{230}Th_{xs}/^{232}Th$ profiles below the first mixed layer.
†"Apparent" sedimentation rate estimated from the ^{210}Pb profile in the second box.
N.D. Not determined.

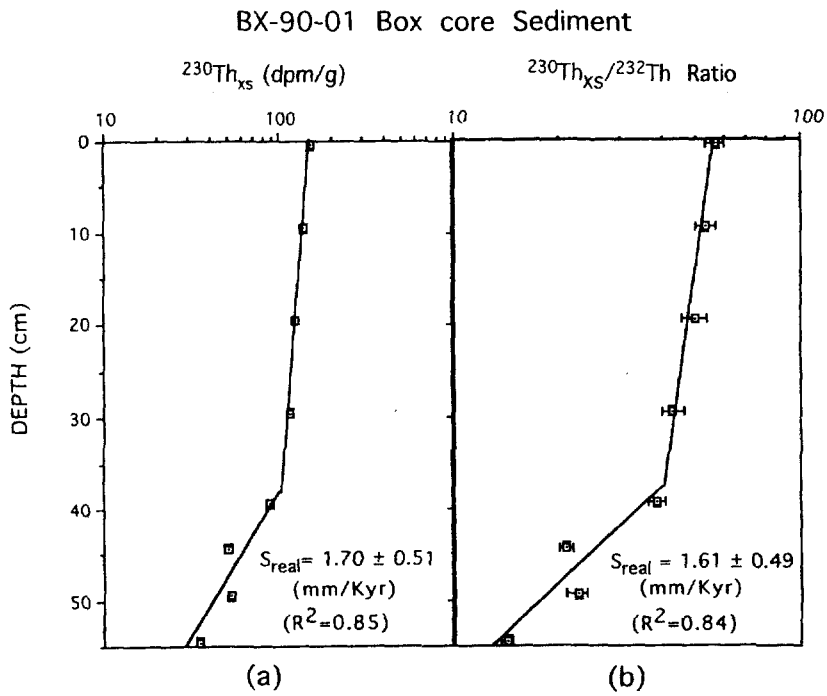

Fig. 9. Plots of $^{230}Th_{xs}$ activity (a) and $^{230}Th_{xs}/^{232}Th$ activity ratio (b) as a function of depth at BX-90-01 core. S=sedimentation rate estimated from all data points. S_{real}=real sedimentation rate calculated from data points below SML (40 cm).

sediment (cm). The errors of activities given in Tables 2 to 6 are 1σ uncertainties based on counting statistics. The sedimentation rates estimated for the cores studied in this study are summarized in Table 7. The uncertainties of the estimation are based on the 1s standard error due to regression and generally less than 20%. Although the geochemical pathways of ^{230}Th and ^{232}Th are different, their chemical behavior during sediment diagenesis should be quite similar. Therefore we prefer using normalized ratios of $^{230}Th_{xs}/^{232}Th$ to $^{230}Th_{xs}$ activities alone in estimating sedimentation rates. Both sedimentation rates estimated from $^{230}Th_{xs}$ and $^{230}Th_{xs}/^{232}Th$ agree each other within the standard errors (Figs. 5, 7 and 9).

In the core BX-90-36, the sedimentation rates estimated to be 0.50±0.10 mm/ky (R^2=0.82) from $^{230}Th_{xs}$ activity and 0.51±0.10 mm/ky (R_2=0.83) from $^{230}Th_{xs}/^{232}Th$ ratio. The two estimates are in an excellent agreement. The "real" sedimentation rate (S_{real}) estimated from the profile of $^{230}Th_{xs}/^{232}Th$ ratio in the lower layer (z>L) is 0.29 0.06 mm/ky, 50 % lower than that obtained from the slope of re-

gression line fitted to all data points.

The sedimentation rates from data points below surface mixed layer (>18.5 cm) in BX-89-15 are estimated to be 0.98±0.36 mm/ky from $^{230}Th_{xs}/^{232}Th$ ratio (Fig. 7). Because the first mixed layer of core BX-89-15 appears down to 18.5 cm (Fig. 8), the " real" sedimentation rate was calculated from slope of regression line fitted to $^{230}Th_{xs}/^{232}Th$ data points within the lower layer. The estimated value of sedimentation rate is 25% lower than that obtained from the regression equation fitted to the entire data points.

The sedimentation rate of BX-90-01 was estimated from the slope of regression fitted to the $^{230}Th_{xs}/^{232}Th$ ratio to be 1.61±0.49 mm/ky (Fig. 9). Excess ^{230}Th activity and $^{230}Th_{xs}/^{232}Th$ ratio show almost flat profiles in surface mixed layer (<40 cm), indicating intense particle mixing. The sedimentation rate estimated from the $^{230}Th_{xs}/^{232}Th$ ratio below surface mixed layer (>40 cm) is 1.61±0.49 mm/ky, a half of the value that obtained from all data points.

The sedimentation rates of BX-90-01 is 5-6 times higher than that of BX-90-36 (Table 7). In the eastern part of the KODOS site, the acoustic basement is fractured and complicated by a number of faults. These small basin and elevation make good condition to develop sedimentary layer (KORDI, 1991). The estimated sedimentation rates are the highest at BX-90-01 site and decrease progressively toward northwest. The analysis of seismic profiles in the KODOS area shows that sedimentary layers thin gradually northward (Jeong *et al.*, 1988).

Particle mixing rates

The evidence of particle mixing appears in excess ^{210}Pb profile. Since the half life of ^{210}Pb ($t_{1/2}$=22.3 y) is much shorter than that of ^{230}Th ($t_{1/2}$=75,200 y), excess-^{210}Pb profile can bear signals of mixing occurred in upper part of sediments. Longer lived nuclides will behave more or less as stable tracers in short time span. Their activities will be essentially constant within the surface mixed layer. This property enables long lived nuclides to be used to estimate the depth of the mixed layer (Cochran, 1982). Because within the second layer mixing is much slower than the above layer, the effect of slow particle mixing occurred in short time span on sedimentation rate can be ignored within the second box. Hence, the "real" sedimentation rate can be obtained from the ^{230}Th profile in deeper part of sediment column slightly affected by particle mixing.

In core BX-90-36, two separate regression lines were drawn by least-squares fitting to the semi-logarithmic plot of excess ^{210}Pb distribution versus core depth (Fig. 6). The two segments of the excess ^{210}Pb distribution profile, intersecting each other at the 21 cm depth, may represent a signal of fast particle mixing above the depth and that of slow mixing below the depth, superimposed on a radioactive decay profile of ^{210}Pb. The "real" sedimentation rate was estimated to be 0.29 mm/ky using the $^{230}Th_{xs}/^{232}Th$ ratio at BX-90-36 (Table 2). The apparent sedimentation rate was calculated to be 0.17 cm/y (R^2= 0.97) from excess ^{210}Pb profile in the second box (below 21 cm). The mixing coefficient for the first (D_1) was estimated to be 22.5 cm^2/y and that in second box (D_2) to be 0.93 cm^2/y using the "real" sedimentation rate of 0.29 mm/ky (Table 7)

Two separate regression lines, representing the first and second mixing layers, were drawn by least-squares fitting to the semi-logarithmic plot of excess ^{210}Pb distribution of BX-89-15 (Fig. 8). The "real" sedimentation rate was estimated to be 0.98 mm/ky using the $^{230}Th_{xs}/^{232}Th$ ratio at BX-89-15 (Table 4). The apparent sedimentation rate was calculated to be 0.16 cm/y (R_2=0.98) from the excess ^{210}Pb activities in the second box (below 18.5 cm). D_1 was estimated to be 6.16 cm^2/y and D_2 to be 0.83 cm^2/y (Table 7).

Although D_2 values are smaller orders of magnitude than D_1, the particle mixing process still exists in the second box. The bioturbation in the second box could have influenced on the "real" sedimentation rate on the contrary to our assumption of no particle mixing within the box. The sedimentation rates determined from the Equatorial Pacific cores using excess ^{230}Th below the mixed layer are 1.5~3.0 mm/ky (DeMaster and Cochran , 1982).

Table 8. Results of sensitivity test of bological mixing rates. The variation of D_1 and D_2 was checked as we changed the sedimentation rates

	BX-90-36			BX-89-15		
	S_{real}*0.1	S_{real}	S_{real}*10	S_{real}*0.1	S_{real}	S_{real}*10
S_{real}(mm/ky)	0.029	0.29	2.9	0.098	0.98	9.8
D_1(cm^2/y)	22.49	22.49	22.48	6.161	6.160	6.147
D_2(cm^2/y)	0.9322	0.9321	0.9306	0.8257	0.8253	0.8207

Also, the sedimentation rates around this study area were reported to be less than 1 mm/ky (Piper and Williamson, 1977). We performed a sensitivity test by checking the variation of D_1 and D_2 as we change the sedimentation rates, S_{real}. We calculated the D_1 and D_2 values in two cases: i) the sedimentation rates are ten times, ii) a tenth our the estimated values (Table 8). Although the sedimentation rates change a hundred-fold from 0.029 mm/ky to 2.9 mm/ky in the BX-90-36 core and from 0.098 mm/ky to 9.8 mm/ky in the BX-89-15 core, D_1 and D_2 values in the both cores show no significant variation (Table 8). Therefore, we conclude that the variation of the real sedimentation rates in the second box has negligible influence on the bioturbation rates (D_1 and D_2).

The particle mixing coefficients for KODOS area fall in the range of 22.5~6.16 cm^2/y in the first mixed layer and 0.93~0.83 cm^2/y in the second layer. Our estimates for the first box mixing coefficients (D_1) are either in the same order of magnitude or one order lower than those calculated for the Peru continental margins (4.2 cm^2/y) (Kim and Burnett, 1988) and nearshore (50~400 cm^2/y) (Berner, 1980). However, they are one or two order of magnitude higher than those calculated from deep-sea sediments of the Equatorial Pacific (0.2~0.4 cm^2/y) (DeMaster and Cochran, 1982) indicating the intensive particle mixing in the KODOS site. Our estimates of the second box mixing coefficient (D_2) are in the same order of magnitude as those measured for deep-sea sediment (DeMaster and Cochran, 1982).

The sediments in the KODOS area are divided into Units A and B, based on color, radiolarian fossils, and lithology (Jeong, 1993; Jung, 1994). The Unit A is pale brown, homogeneous, intensively bioturbated and is assigned to the late Quaternary. The Unit B is dark brown in color, less bioturbated and is allotted to the Tertiary by radiolarian fossils. The color boundary appear at the transitional zone between units A and B, which is interpreted as the hiatus between the late Quaternary and the Tertiary (Jung, 1994). The depths of the color boundary layers in the sediment cores are in excellent agreement with the first mixed layer depths (L) interpreted from the profiles of the excess ^{230}Th and the excess ^{210}Pb in our cores (Fig. 5-8).

CONCLUSIONS

Two estimates of sedimentation rates, determined by $^{230}Th_{xs}$ and $^{230}Th_{xs}/^{232}Th$ dating methods for 3 cores, were in very good agreement. The estimated sedimentation rate at the southeastern part of the study area (BX-90-01) was 1.61 ± 0.49 millimeters per thousand years. At the northwestern part of the KODOS site (BX-89-15 and BX-90-36), the sedimentation rates were estimated to be in the range of 0.29~0.98 mm/ky. Excess ^{230}Th activities and $^{230}Th_{xs}/^{232}$Th ratios show profiles of constant values in the top 10 cm of sediment cores, considered to be generated by biological particle mixing.

A "two-box" advection diffusion steady state mixing model has been applied to the distribution profiles of excess ^{210}Pb in sediment core samples collected from BX-89-15 and BX-90-36 in order to estimate particle mixing rates in the upper and the lower layers. Particle mixing coefficients were estimated to be in the range of 6.16~22.5 cm^2/y for the upper mixed layer and 0.8~0.9 cm^2/y for the lower layer. Active biological particle mixing occurs in the upper 18~20 cm of the sediment core in the study area. Active particle mixing in surface sed-

iment may play one of the important roles in keeping manganese nodules from being buried in sediments.

ACKNOWLEDGMENT

We thank Dr. J.K. Kang and Dr. K.S. Jeong for their approval of using sediment samples. We are grateful to KORDI scientists and the officers and crew of the R/V Farnella for their assistance in the field work part of this research. We wish to express gratitude to the members of the Marine Radiochemistry Laboratory, Oceanography Department of Chungnam National University for their assistance in laboratory works. Also we wish to express our thanks to Drs. G.H. Hong and J.K. Kang for the invaluable critics and reviews on the manuscripts.

REFERENCES

Aller, R. C. and DeMaster, D. J., 1984. Estimates of particle flux at the deep-sea floor using 234Th/238U disequilibrium, *Earth Planet. Sci. Lett.*, **67**: 308-318.

Aller, R. C. and Cochran, J. K., 1976. The $^{234}Th/^{238}U$ disequilibrium in near-shore sediments: particle reworking and diagenetic time scales, *Earth Planet. Sci. Lett.*, **29**: 37-50.

Anderson, R. F. and Fleer, A. P., 1982. Determination of natural actinides and plutonium in marine particulate material, *Anal. Chem.*, **54**: 1142-1147.

Benninger, L. K. and Krishnaswami, S., 1981. Sedimentary processes in the inner New York Bight: evidence from excess ^{210}Pb and $^{239,240}Pu$, *Earth Planet. Sci. Lett.*, **53**: 158-174.

Broecker, W. S. and Peng, T. -H., 1982. Tracer in the sea. Eldigio Press, Palisades, New York, 690p.

Cochran, J. K., 1985. Particle mixing rates in sediments of the eastern equatorial Pacific: evidence from ^{210}Pb, $^{239,240}Pu$ and 137Cs distribution of MANOP sites. *Geochem. Cosmochim. Acta*, **99**: 1195-1210

Cochran, J. K., 1982. The oceanic chemistry of U- and Th-series nuclides, in: *Uranium Series Disequilibrium, Applications to Environmental Problems*, (ed. M. Ivanovich and R. S. Harmon), Clarendon Press, Oxford: 459-496.

DeMaster, D. J. and Cochran, J. K., 1982. Particle mixing rates in deep-sea sediments determined from excess ^{210}Pb and ^{32}Si profiles, *Earth Planet. Sci. Lett.*, **61**: 257-271.

Goldberg, E. D., 1963. The ocean as a chemical system, In: *The sea*, (ed. M. N. Hill), New York, Interscience, **2**: 3-25.

Goldberg, E. D. and Koide M., 1962. Geochronological studies of deep sea sediments by the thorium-ionium method. *Geochem. Cosmochim. Acta*, **26**: 417-450.

Huh, C. A., 1982. Radiochemical and chemical studies of manganese nodules from three sedimentary regimes in the North Pacific. Ph.D. Thesis, University of Southern California, Los Angeles, 305 pp.

Jeong, K. S., Han, S. J. and Kim, S. R., 1988. Acoustic stratigraphy and sedimentary processes in the KONOD-1 area between the Clarion and Clipperton Fracture Zones, northeastern Equatorial Pacific. *Jour. Oceanogr. Soc. Kor.* **23**: 25-40

Jeong, K. S., 1993. Sedimentary processes and formation of manganese nodules in the Korea Deep Ocean Study (KODOS) area, western Clarion-Clipperton fracture zones, Northeast Equatorial Pacific. Ph.D thesis, Seoul Nat. Univ. 300pp.

Joshi, S. R, 1985 Determination of thorium-228, 230, 232, in sediments by anion exchange and nuclear spectrometer, *Anal. Chem. 57, 1023-1026*

Jung, H. S, Kang, J. K., Jeong, K. S. and Shin, D. H., 1991. Geochemical characteristics of light yellow brown surface sediments and dark brown colored subsurface sediments in KODOS-89 area, western part of Clarion-Clipperton fracture zone in north pacific, *Jour. Oceanogr. Soc. Kor.* **26**: 193-203

Jung, H. S, 1994, Geochemistry of sediments, pore waters, and manganese noldules in KODOS area, western part of Clarion-Clipperton fracture zone in the North Pacific. Ph.D thesis, Seoul Nat. Univ. 281pp.

Kim, K. H. and Burnett, W. C., 1988. Accumulation and biological mixing of Peru margin sediments. In: The Origin of Marine Phosphorites. The Result of the *R. V. Robert D. Conrad* Cruise 23-06 to the Peru Shelf, (ed. W. C. Burnett and P. N. Froelich), *Mar. Geol.*, **80**: 181-194.

Kim, K. H. and Burnett, W. C., 1983. Gamma-ray spectrometric determination of uranium series nuclides in marine phosphorites, *Anal. Chem.*, **55**: 1796-1800.

KORDI, 1992. A study on the strategy for the development of deep seabed mineral resources (III) (Cruise Report). BSPG 000143-542-5, 1-720.

KORDI, 1991. A study on the strategy for the development of deep seabed mineral resources (II) (Cruise Report). BSPG 000118-369-5, 1-1093.

KORDI, 1990. A study on the strategy for the development of deep seabed mineral resources (I) (Cruise Report). BSPG 00094-296-5, 1-1093.

KORDI, 1987. Guide to marine mineral resources. Korean Ocean Research and Development Institute. BSPG 00088-138-5

KORDI, 1986. A further study on the manganese nodules, sediments and geomagnetism of the KONOD-1 site : Northeastern central pacific. BSPG 00066-99-5, pp.1-219

Krishnaswami, S., Benninger, L. K., Aller, R. A. and Von Dam, K. L., 1980. Atmospherically-derived ra-

dionuclides as tracers of sediment mixing and accumulation in near-shore marine and lake sediments: evidence from 7Be, ^{210}Pb and ^{239,240}Pu, *Earth Planet. Sci. Lett.*, **47**: 307-318.

Lynn, D. C. and Bonatti, E., 1965. Mobility of manganese in diagenesis of deep-sea sediments, *Mar. Geol.*, **3**: 457-474.

Piper, D. Z. and Fowler B., 1980, New constraint on the maintenance of Mn nodules at the sediment surface, Nature, v. 286, no. 5776, pp. 880-883

Piper, D. Z. and Williamson, M. E., 1977, Composition of Pacific ocean ferromanganese nodules, *Mar. Geol.*, **23**: 285-303.

Santschi, P. H., Li, Y. H., Bell J., Trier R. M. and Kautaluk K., 1986. Pu in coastal marine environments, *Earth Plane. Sci. Lett.*, **51**: 248-265.

Accepted August 3, 1995